Membrane shape as a reporter for applied forces

Heun Jin Lee, Eric L. Peterson, Rob Phillips
California Institute of Technology, 1200 E. California Blvd, Pasadena, CA 91125

William S. Klug
*Department of Mechanical and Aerospace Engineering and Program in Biomedical Engineering,
University of California, Los Angeles, CA 90095*

Paul A. Wiggins*
Whitehead Institute for Biomedical Research, 9 Cambridge Center, Cambridge, MA 02142†
(Dated: May 9, 2008)

Recent advances have enabled three-dimensional reconstructions of biological structures in vivo, ranging in size and complexity from single proteins to multicellular structures. In particular, tomography and confocal microscopy have been exploited to capture detailed three-dimensional conformations of membranes in cellular processes ranging from viral budding and organelle maintenance to phagocytosis. In spite of the wealth of membrane structures available, there is as yet no generic, quantitative method for their interpretation. We propose that by modeling these observed biomembrane shapes as fluid lipid bilayers in mechanical equilibrium, the externally applied forces as well as the pressure, tension and spontaneous curvature can be computed directly from the shape alone. To illustrate the potential power of this technique, we apply an axial force with optical tweezers to vesicles and explicitly demonstrate that the applied force is equal to the force computed from the membrane conformation.

INTRODUCTION

Biomembranes, phospholipid bilayers which form the boundaries of cells and compartmentalize cellular organelles, are intricately and dynamically structured on the sub-micron length scale [1]. The cellular membrane must undergo constant conformational remodeling in diverse cellular processes, ranging from intracellular trafficking (vesiculation and endocytosis) to the biogenesis of membrane-bound organelles. These intricate structures are precisely regulated and are integral to organelle and cellular function [1]. Recent advances in microscopy have resulted in an increasingly detailed structural picture of cellular membranes and organelles. For instance, cryo-electron tomography has enabled the reconstruction of high-resolution, three-dimensional models of organelle structure (the mitochondrion [2], the Golgi apparatus [3], the endoplasmic reticulum [3] and the organelles of an entire cell [4]) as well as HIV viral entry [5], the architecture surrounding synaptic vesicles [6], and the endocytotic machinery [7]. Similarly, confocal and "super-resolution" fluorescence microscopy have emerged as a powerful tools for the capture of three-dimensional cellular structure [8–10].

Although these microscopy-based membrane structures have led to revolutions in our qualititative understanding of membrane morphology, no general technique exists as yet for their quantitative analysis. In particular, a number of mechanisms have been identified which deform the membrane [1]: the aggregation of transmembrane proteins [11, 12], active remodeling by molecular motors [13–15], assembly and disassembly of cytoskele-

tal filaments [16–18], and direct or indirect scaffolding by proteins [19, 20]. However, the study of these mechanisms has been limited, especially *in vivo*. For instance, it has long been postulated that the mechanics of the membrane plays an important role in the aggregation of membrane proteins [21], and recent simulations have also lent support to this idea [22]. In this case, knowledge of the mechanical forces applied by aggregating membrane proteins to an experimentally-observed membrane structure would shed further light on their size, distribution and mutual interaction. The quantitative measurement of the location and magnitude of the forces applied by cellular machinery promises to yield important insights into the detailed mechanisms of membrane remodeling processes, from the life cycle of a membrane-bound virus to the scaffolding underlying organelle structure.

In this paper, (i) we propose a quantitative technique for computing the external forces applied to a membrane from the observed membrane conformation; (ii) we apply this method to explicitly demonstrate that conformation-based force computation agrees with the applied force in an optical-tweezer driven membrane-tether pulling experiment. The conformation-based method of force measurement that we describe here represents a meeting of theoretical, computational and experimental approaches, demonstrating that the Helfrich-Canham-Evans theory of lipid bilayers allows measurement of mechanical force from an observed membrane conformation in a sub-piconewton optical tweezing experiment. Finally, (iii) we argue that the symmetric, two-dimensional implementation demonstrated here may be extended with specialized state-of-the-art finite element methods [23] to calculate the forces applied to arbitrary membrane shapes
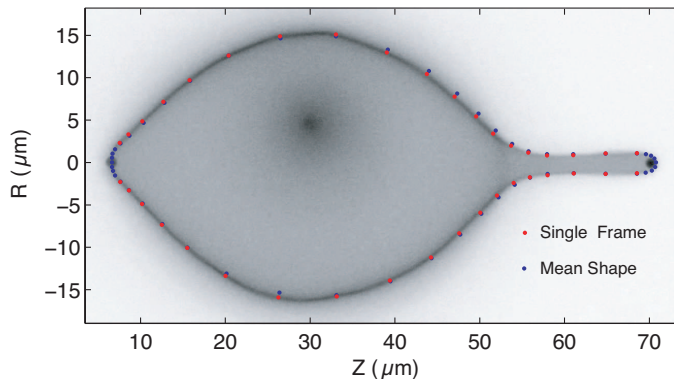
FIG. 1: **Capturing the membrane conformation:** A fluorescence image of a vesicle from a force-extension series. The vesicle conformation is represented as a cubic spline. The positions of the control vertices are fit from the fluorescence profile. The red vertices were traced from the fluorescence image shown in the figure; the blue vertices correspond to a trace of the mean of the fifty images at this extension. The deviation of the instantaneous structure (red) from the mean structure (blue) is a consequence of the long-wavelength thermal undulations.

measured via electron tomography or fluorescence microscopy. We argue that these techniques may be extended to describe the forces shaping *in vivo* biomembranes although the interpretation of these structures is complicated by the the heterogeneity of the biomembranes themselves [24].

THEORY AND METHODS

The mechanical theory of fluid-phase lipid membranes has been the subject of extensive study [24, 25] and experiments suggest that the response of membranes to the application of force is well-approximated by the theory of Helfrich, Canham and Evans [26–28]. The Helfrich model describes the conformational energy of the membrane in terms of an energy density ε that is a function of the local shape of the membrane:

$$\varepsilon = \tfrac{1}{2}k_C \left(S^2 - 2CS \right), \qquad (1)$$

where S is the sum of the principal curvatures with associated bending modulus k_C and C is the spontaneous curvature. The spontaneous curvature describes the spontaneous bending of the membrane induced by asymmetries in the lipid composition or chemical environment of the individual leaflets. The elastic force density applied by the membrane is determined by performing the first variation of the Helfrich energy [29]. Since the membrane is fluid in-plane [30, 31], the equilibrium elastic force per unit area is in the direction perpendicular to the membrane:

$$f_\perp = S\alpha - p - k_C \left[\nabla^2 S - 2K \left(S - C \right) + \tfrac{1}{2}S^3 \right], \quad (2)$$

where K is the Gaussian curvature (the product of the principal curvatures); the parameters α and p are the tension and pressure difference over the membrane respectively. The local force density depends on the local membrane geometry, which is directly observable, and three Lagrange multipliers: the pressure, tension, and spontaneous curvature, which must be determined. To compute these unknown Lagrange multipliers, we apply the *Proximal Equilibrium Approximation* which uses a maximum-likelihood principle to determine the values of pressure, tension and spontaneous curvature which predict an equilibrium conformation closest to the observed conformation[1].

The total elastic force applied by a region of the membrane is calculated as the integral over the force density in that region. Due to the mathematical form of the Helfrich energy, the total elastic force (applied by the membrane) can also equivalently be computed as a contour integral on the region boundary[2] [32]. Evaluating the force at the boundary has two significant practical advantages over the direct integration of the predicted force density: (i) the boundary integral depends on lower-order numerical derivatives, making it less sensitive to experimental noise, and (ii) regions of the membrane where the structure is poorly determined can be bypassed. We term the force measured in this way from the membrane morphology the "conformational force", since it is based purely on information contained in the observed shape of the membrane.

Force-induced membrane tether formation [33, 34] provides a convenient test of the conformational force computation: a known force, applied to an optically trapped bead, can be directly compared to the conformational force. The progression of vesicle shapes in our experiment as the tether forms is illustrated by the membrane conformations shown in gray in the background of Fig. 3. As the axial force is increased, the vesicle first assumes an elongated shape before reaching a transition in which a cylindrical tether forms at one end of the vesicle. This transition is seen in reverse in the retraction phase of the experiment. In our experiment, forces were applied via optically trapped beads to DOPC giant unilamellar vesicles. The streptavidin-coated beads were linked to the vesicles via biotin-labeled lipids. The bending modulus k_C for DOPC is 0.85×10^{-19} J [35]. The structure of the vesicles in these experiments is captured via fluorescence microscopy and is limited in two respects: (i) the observed membrane shape is based on imaging the mid-plane of the vesicle and axial symmetry must

---

[1] The Proximal Equilibrium Approximation is described in more detail in the Supplement.
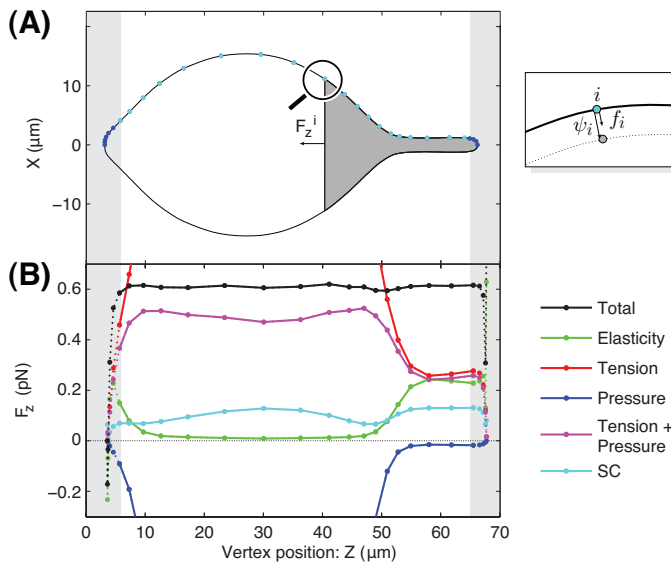[2] See the Supplement for an explanation of this technique and additional references.

FIG. 2: **The Proximal Equilibrium Approximation.**
(A) Vesicle conformation: The axisymmetric vesicle conformation is represented as a cubic spline. The control vertices are shown as points along the contour. In order to find the pressure, tension and spontaneous curvature of the membrane, we choose initial values of these parameters which produce a trial membrane configuration. On the right we show a magnified view of the observed membrane shape (solid curve) as well as the trial shape (dotted line) near control vertex i where the displacement between the vertex in the observed shape (light blue) and the trial shape (light gray) is labeled as ψ_i. We minimize the mean square displacements ψ_i with respect to the trial values of pressure, tension and spontaneous curvature in order to form a best estimate for the values of these parameters. During the minimization we exclude the regions in the proximity of the bead attachment points, shaded in gray on the left and right, where the membrane shape cannot be resolved with sufficient precision to make reliable force estimates.
(B) Summed force: The summed force at vertex i, F_z^i, is the sum of the z components of the vertex forces in the dark-gray region which excludes vertices with $z < z_i$. F_z^i is the total force applied by the right hand side of the vesicle in the z direction. In this panel we plot the total summed force (black) which, as expected, is approximately constant throughout the body of the vesicle, since the forces are applied only at the poles of the vesicle. The summed force is also shown decomposed into individual contributions from pressure, tension, spontaneous curvature and bending elasticity.

be assumed to construct the three-dimensional structure, and (ii) the resolution of the membrane structures is the optical-diffraction limit.

In a typical experiment, fifty fluorescent images were captured at each step in an extension series[3]. An exten-

sion series typically consisted of between fifty and sixty steps split between extension and retraction, with a step size of roughly 1.5 μm. The integration time was chosen to give sufficient pixel statistics to allow the contour of the membrane in each image to be traced independently. The vesicle conformation is represented as a cubic spline with control vertices as shown in Fig. 1. The position of the vertices in the direction parallel to membrane surface was chosen by hand; the position in the direction perpendicular to the surface was fit to the fluorescence profile independently in each frame.[4] In our analysis, we shall assume that the vesicle is axially symmetric so that the observed cross-sectional structure determines the entire vesicle structure. This approximation is excellent at large extensions, but breaks down at low force.

RESULTS

A typical single fluorescence image of a tethered vesicle is shown in Fig. 1 together with the vertices traced from the image frame. The mechanics of the membrane should be independent of a particular vertex representation: observable physical quantities cannot depend on the positions of the control vertices in the direction parallel to the membrane surface. The individual vertex forces f_i do depend on the vertex position for two reasons: the vertex positions control the effective area of each vertex, and the vertex force depends on the fourth derivative of the vertex positions. On the other hand, the equilibrium displacement ψ_i, the estimated displacement to the equilibrium conformation at each vertex, is approximately independent of the effective vertex area and suppresses the derivative noise since high-frequency modes have a high stiffness[5]. (See Fig. 2, panel A.) To implement the *Proximal Equilibrium Approximation*, we therefore minimized the square of the equilibrium displacements at each vertex to determine the Lagrange multipliers. Panel A of Fig. 2 shows that the measured conformation closely matches the estimated equilibrium conformation for the optimized Lagrange multipliers (pressure: 3.4 ± 0.2 mPa, tension: 7.4 ± 0.5 $k_B T/\mu m^2$, and spontaneous curvature: -0.27 ± 0.10 μm^{-1}) determined by the *Proximal Equilibrium Approximation*. In spite of the apparent representation dependence of the vertex forces, we find that the integrated force results in consistent force predictions. In panel B of Fig. 2, we plot the integrated force for slices of the vesicle perpendicular to the z-axis.

---

[3] All the structures for the data set discussed in the text are shown in the Supplemental Material.

[4] The capture of the instantaneous structure allows the comparison of the thermal undulations to the predicted stiffness matrix [36].
[5] We demonstrated the representation independence by making independent tracings of each data set which resulted in nearly identical measurements of physically observable quantities. (For more information see the Supplement.)

As expected, this force is nearly constant throughout the body of the vesicle, a key consistency condition since forces are applied only at the axial poles of the vesicle.

To demonstrate the power of conformation force computation, we explicitly show that the conformational forces correctly predict the applied force as a tether is pulled from a vesicle by an optical tweezer. In order to resolve the structure of tethered vesicles by light microscopy, the force at which tethers formed had to be less than 2 pN, implying that the undeformed vesicles had a large excess of area (low tension). In Fig. 3, we compare the conformational forces to the applied force for a tether extension and retraction. (The corresponding optimized Lagrange multipliers are plotted in the Supplement.) We measure a mean relative error of 10% for forces in the range of 0.2 to 1 pN, showing that the applied and conformational force are in both qualitative and quantitative agreement in that range. The optical tweezing force measurements suffered from two important shortcomings in the sub-piconewton regime: (i) Sub-piconewton force measurements are generically susceptible to drift. (ii) The vesicles themselves were also found to weakly scatter the trapping beam, resulting in anomalous force signals during large-scale changes in vesicle structure. For instance, only data sets where the force sensor bead was not positioned on the end of the tether were found to result in consistent force traces. The mismatch between conformational and applied forces appears to increase towards the end of the retraction, consistent with both trap drift and membrane conformation induced beam scattering. Our analysis also revealed limitations in the conformational force technique. For very low forces, the conformational force is limited by the determination of the Lagrange multipliers. At high force, the conformational force is limited by diffraction as the typical length scale of the neck of the tether shrinks below that limit.

DISCUSSION

The central theme of this work is the development and validation of a framework that is *generally applicable* to the computation of mechanical forces applied to a membrane of arbitrary shape, including the contributions of pressure, tension, and spontaneous curvature. Although the formation of membrane tethers is both well-known and well-studied in the membrane mechanics literature [37–40], it nevertheless provides a convenient proof-of-principle experiment where both the force, applied by the optical trap, and the membrane conformation are known simultaneously. While our measurements have been restricted to structures derived from light microscopy, the full potential of the conformation-based force measurement technique lies in the fully three-dimensional structures captured via tomography or confocal microscopy. Computational techniques to analyze three-dimensional
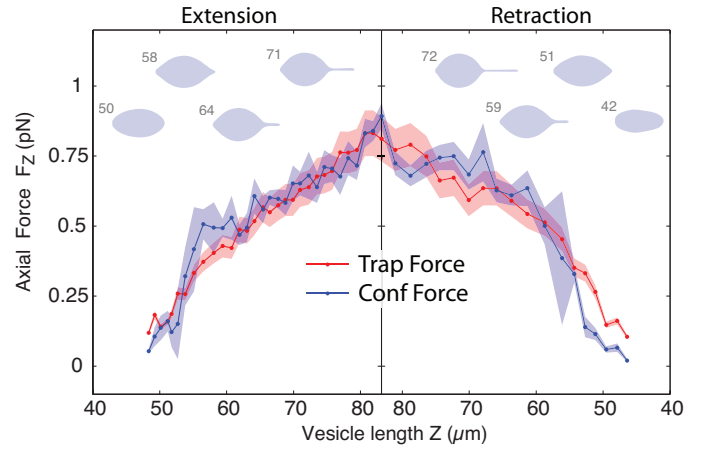
FIG. 3: **Comparison of the applied and conformational force.** The computed conformational force (blue curve) and the applied trapping force (red curve) are in both qualitative and quantitative agreement from 0.1 to 1 pN. The shaded regions are error in the trapping force and the r.m.s. variation in the conformational force, respectively. Note that the x-axis orientation has been inverted in the retraction data. **Inset:** Membrane conformations as a function of axial length (μm).

membrane conformations have been described elsewhere [23] and would extend our framework in a natural way to general membrane structures.

We expect conformational force calculations to be a powerful tool for analyzing *in vitro* membrane conformation, but the most exciting potential applications are the analysis of *in vivo* membrane remodeling processes. We can estimate the spatial resolution required to image structures of interest by examining the dependence of the force at tether formation on curvature.[6] Given an applied force F, the approximate scale of membrane bending R is given by $R \sim 2\pi k_C/F = 0.4 \ (1 \text{ pN}/F) \ \mu$m. Since the typical protein-scale biological forces are several pN, the conformational force technique will be most powerful in the analysis of structure captured at resolutions higher than the optical diffraction limit. There are no other experimental tools which allow the measurement of forces applied to membranes *in vivo*. Previous experiments have been limited to the extrusion of tethers from living cells but these experiments probe deformations on scales beyond those normally experienced by the cell in membrane remodeling processes [41, 42].

The greatest challenge to extending these techniques to *in vivo* biomembranes is the heterogeneity of the biomembranes themselves. The analysis of membranes with phase boundaries adds considerable complexity to the

---

[6] The tether-force equation is the exact equilibrium force required to support a tether radius R in the absence of spontaneous curvature [38].

problem [24]. In spite of these difficulties, the technique described here exhibits a number of powerful properties which may help to circumvent these potential pitfalls. For instance, even in a case where the membrane structure cannot be resolved in a localized region because of the presence of a large protein scaffold or lipid raft, we may still measure forces provided a surrounding region of fluid membrane exists, since the boundary force method only requires knowledge of the shape of the membrane on the *boundary* of a region of interest. This feature is also essential for the analysis of data from electron tomography which are typically incomplete because of the "missing wedge" artifact.

Another potentially daunting challenge is the determination of the Lagrange multipliers for *in vivo* systems where the number of contact points is potentially much greater than the tethered vesicles discussed in this paper. But the determination of three Lagrange multipliers using the *Proximal Equilibrium Approximation* is a peculiarity of the *in vitro* tether formation process where the membrane undergoes a dramatic conformational change on the same scale as the vesicle itselfFor most biological membrane remodeling examples, where the membrane mechanics is relevant, the pressure is negligibly small. Furthermore, studies suggest that the tension (and spontaneous curvature) may be a regulated property of many cytoplasmic and organelle membranes [41]. When the Lagrange multipliers are known or determined, the forces can be directly computed.

In spite of these potential limitations, quantitative analysis of the membrane structure holds the promise of probing the forces and structural elements that are at work in biological membrane remodeling processes which intricately shape biological membranes and are integral to organelle and cellular function. For instance, quantitative structural analysis could reveal the structural nature of the scaffolds that dynamically maintain and remodel organelle membranes. Are scaffolds necessary to maintain the structure of mitochondrial cristae and cristae junctions in the inner membrane? What is the structural basis for the creation and maintenance of the inter-connected fenestrations in the Golgi apparatus and endoplasmic reticulum? Quantitative structural analysis could also be exploited to quantitatively test the aggregation-driven models of HIV1 viral particle budding. Are the GAG protein aggregates structurally sufficient to give rise to the observed cytoplasmic bud conformations? The techniques discussed in this paper demonstrate that the three-dimensional structures captured by cryo-EM tomography and confocal and fluorescence microscopy can be transformed into quantitative structural models that report forces and potentially the structural nature of cellular processes *in vivo*.

---

* Electronic address: wiggins@wi.mit.edu
† URL: http://wiggins.wi.mit.edu/

[1] Harvey T McMahon and Jennifer L Gallop. Membrane curvature and mechanisms of dynamic cell membrane remodelling. *Nature*, 438(7068):590–596, 2005.

[2] T G Frey and C A Mannella. The internal structure of mitochondria. *Trends Biochem Sci*, 25(7):319–324, 2000.

[3] M S Ladinsky, D N Mastronarde, J R McIntosh, K E Howell, and L A Staehelin. Golgi structure in three dimensions: functional insights from the normal rat kidney cell. *J Cell Biol*, 144(6):1135–1149, 1999.

[4] Gregory P. Henderson, Lu Gan, and Grant J. Jensen. 3-d ultrastructure of o. tauri: Electron cryotomography of an entire eukaryotic cell. *PLoS ONE*, 2(8):e749, Aug 2007.

[5] Rachid Sougrat, Alberto Bartesaghi, Jeffrey D Lifson, Adam E Bennett, Julian W Bess, Daniel J Zabransky, and Sriram Subramaniam. Electron tomography of the contact between t cells and siv/hiv-1: implications for viral entry. *PLoS Pathog*, 3(5):e63, 2007.

[6] M L Harlow, D Ress, A Stoschek, R M Marshall, and U J McMahan. The architecture of active zone material at the frog's neuromuscular junction. *Nature*, 409(6819):479–484, 2001.

[7] Yifan Cheng and Thomas Walz. Reconstructing the endocytotic machinery. *Methods Cell Biol*, 79:463–487, 2007.

[8] Samuel T Hess, Travis J Gould, Manasa V Gudheti, Sarah A Maas, Kevin D Mills, and Joshua Zimmerberg. Dynamic clustered distribution of hemagglutinin resolved at 40 nm in living cell membranes discriminates between raft theories. *Proc Natl Acad Sci U S A*, 104(44):17370–17375, 2007.

[9] D Gerlich, J Beaudouin, M Gebhard, J Ellenberg, and R Eils. Four-dimensional imaging and quantitative reconstruction to analyse complex spatiotemporal processes in live cells. *Nat Cell Biol*, 3(9):852–855, 2001.

[10] Bo Huang, Wenqin Wang, Mark Bates, and Xiaowei Zhuang. Three-dimensional super-resolution imaging by stochastic optical reconstruction microscopy. *Science*, 319(5864):810–813, 2008.

[11] H C Fertuck and M M Salpeter. Localization of acetylcholine receptor by 125i-labeled alpha-bungarotoxin binding at mouse motor endplates. *Proc Natl Acad Sci U S A*, 71(4):1376–1378, 1974.

[12] Nigel Unwin. Refined structure of the nicotinic acetylcholine receptor at 4a resolution. *J Mol Biol*, 346(4):967–989, 2005.

[13] Gerbrand Koster, Martijn VanDuijn, Bas Hofs, and Marileen Dogterom. Membrane tube formation from giant vesicles by dynamic association of motor proteins. *Proc Natl Acad Sci U S A*, 100(26):15583–15588, 2003.

[14] Enrique Rodriguez-Boulan, Geri Kreitzer, and Anne Musch. Organization of vesicular trafficking in epithelia. *Nat Rev Mol Cell Biol*, 6(3):233–247, 2005.

[15] R D Vale and H Hotani. Formation of membrane networks in vitro by kinesin-driven microtubule movement. *J Cell Biol*, 107(6 Pt 1):2233–2241, 1988.

[16] C M Waterman-Storer, R A Worthylake, B P Liu, K Burridge, and E D Salmon. Microtubule growth activates rac1 to promote lamellipodial protrusion in fibroblasts. *Nat Cell Biol*, 1(1):45–50, 1999.

[17] M P Sheetz. Cell control by membrane-cytoskeleton adhesion. *Nat Rev Mol Cell Biol*, 2(5):392–396, 2001.

[18] Maria Dolores Ledesma and Carlos G Dotti. Membrane and cytoskeleton dynamics during axonal elongation and stabilization. *Int Rev Cytol*, 227:183–219, 2003.

[19] Bruno Antonny, Pierre Gounon, Randy Schekman, and Lelio Orci. Self-assembly of minimal copii cages. *EMBO Rep*, 4(4):419–424, 2003.

[20] B Razani and M P Lisanti. Caveolins and caveolae: molecular and functional relationships. *Exp Cell Res*, 271(1):36–44, 2001.

[21] R Bruinsma and P Pincus. Protein aggregation in membranes. *Current opinion in solid state & materials science*, 1(3):401–406, 1996.

[22] Benedict J Reynwar, Gregoria Illya, Vagelis A Harmandaris, Martin M Muller, Kurt Kremer, and Markus Deserno. Aggregation and vesiculation of membrane proteins by curvature-mediated interactions. *Nature*, 447(7143):461–464, 2007.

[23] Feng Feng and William S. Klug. Finite element modeling of lipid bilayer membranes. *Journal of Computational Physics*, 220(1):394–408, 2006.

[24] Tobias Baumgart, Samuel T Hess, and Watt W Webb. Imaging coexisting fluid domains in biomembrane models coupling curvature and line tension. *Nature*, 425(6960):821–4, 2003.

[25] U. Seifert. Configurations of fluid membranes and vesicles. *Advances in Physics*, 46(1):13–137, Jan-Feb 1997.

[26] P B Canham. The minimum energy of bending as a possible explanation of the biconcave shape of the human red blood cell. *J Theor Biol*, 26(1):61–81, 1970.

[27] E A Evans. Bending resistance and chemically-induced moments in membrane bilayers. *Biophysical Journal*, 14:923–931, 1974.

[28] W Helfrich. Elastic properties of lipid bilayers: theory and possible experiments. *Z. Naturforsch.*, 28(11):693–703, 1973.

[29] J T Jenkins. Static equilibrium configurations of a model red blood cell. *J Math Biol*, 4(2):149–69, 1977.

[30] S J Singer and G L Nicolson. The fluid mosaic model of the structure of cell membranes. *Science*, 175(23):720–731, 1972.

[31] Akihiro Kusumi, Chieko Nakada, Ken Ritchie, Kotono Murase, Kenichi Suzuki, Hideji Murakoshi, Rinshi S Kasai, Junko Kondo, and Takahiro Fujiwara. Paradigm shift of the plasma membrane concept from the two-dimensional continuum fluid to the partitioned fluid: high-speed single-molecule tracking of membrane molecules. *Annu Rev Biophys Biomol Struct*, 34:351–378, 2005.

[32] R. Capovilla and J. Guven. Stress and geometry of lipid vesicles. *Journal of Physics-Condensed Matter*, 16(22):S2187–S2191, Jun 2004.

[33] Deborah Kuchnir Fygenson, John F. Marko, and Albert Libchaber. Mechanics of microtubule-based membrane extension. *Physical Review Letters*, 79(22):4497–4500, 1997.

[34] Damien Cuvelier, Imre Derenyi, Patricia Bassereau, and Pierre Nassoy. Coalescence of membrane tethers: experiments, theory, and applications. *Biophys J*, 88(4):2714–26, 2005.

[35] W Rawicz, K C Olbrich, T McIntosh, D Needham, and E Evans. Effect of chain length and unsaturation on elasticity of lipid bilayers. *Biophys J*, 79(1):328–339, 2000.

[36] Heun Jin Lee, Eric Lee Peterson, and P A Wiggins. Manuscript in preparation, 2008.

[37] R E Waugh and R M Hochmuth. Mechanical equilibrium of thick, hollow, liquid membrane cylinders. *Biophys J*, 52(3):391–400, 1987.

[38] R E Waugh, J Song, S Svetina, and B Zeks. Local and nonlocal curvature elasticity in bilayer membranes by tether formation from lecithin vesicles. *Biophys J*, 61(4):974–82, 1992.

[39] V Heinrich, B Bozic, S Svetina, and B Zeks. Vesicle deformation by an axial load: from elongated shapes to tethered vesicles. *Biophys J*, 76(4):2056–71, 1999.

[40] Thomas R Powers, Greg Huber, and Raymond E Goldstein. Fluid-membrane tethers: minimal surfaces and elastic boundary layers. *Phys Rev E*, 65(4 Pt 1):041901, 2002.

[41] Arpita Upadhyaya and Michael P Sheetz. Tension in tubulovesicular networks of golgi and endoplasmic reticulum membranes. *Biophys J*, 86(5):2923–8, 2004.

[42] J P Mills, L Qie, M Dao, C T Lim, and S Suresh. Nonlinear elastic and viscoelastic deformation of the human red blood cell with optical tweezers. *Mech Chem Biosyst*, 1(3):169–180, 2004.

Membrane shape as a reporter for applied forces
Supplemental Material

Heun Jin Lee, Eric L. Peterson, Rob Phillips

California Institute of Technology, 1200 E. California Blvd, Pasadena, CA 91125

William S. Klug

Department of Mechanical and Aerospace Engineering and Program in Biomedical Engineering,
University of California, Los Angeles, CA 90095

Paul A. Wiggins[*]

Whitehead Institute for Biomedical Research, 9 Cambridge Center, Cambridge, MA 02142[†]
(Dated: May 9, 2008)

Contents

[*]Electronic address: wiggins@wi.mit.edu
[†]URL: http://wiggins.wi.mit.edu/

I. THEORY

A. Preliminary definitions

In these calculations, the structure of the membrane $\mathcal{M}$ is described by the embedding map $X : \mathbb{R}^2 \to \mathbb{R}^3$. We use arbitrary local coordinates σ^1 and σ^2 on the membrane. The pull-back metric on the surface is $g_{ij} = \partial_i X^\alpha \partial_j X^\alpha$ where the latin indices will refer to the coordinate system on the membrane, $\mathcal{M}$, and the greek indices will refer to the $\mathbb{R}^3$ embedding space and we use the Einstein convention (sum repeated indices). The measure on the membrane is $\sqrt{g} \equiv \sqrt{\det g_{ij}}$. The curvature is described by the shape operator, and is defined as:

$$\mathbf{S} \equiv -\mathrm{d}X^\alpha \otimes \mathrm{d}n^\alpha, \tag{1}$$

where d is the exterior derivative on $\mathcal{M}$, and n^α is the outward unit normal to the surface. The sum of the principal curvatures is the trace of the shape operator, $S \equiv \mathrm{tr}\, \mathbf{S}$, which is twice the mean curvature H, and the Gaussian curvature is the determinant of the shape operator $K \equiv \det \mathbf{S}$.

B. Helfrich-Canham-Evans theory

The membrane deformation free energy is described by the canonical theory of bilayer membranes, proposed independently by Helfrich, Canham and Evans [6–8]:

$$E = \int_{\mathcal{M}} \mathrm{d}^2\sigma \, \sqrt{g} \left[\tfrac{1}{2} k_C \left(S - C \right)^2 + k_G K \right], \tag{2}$$

where the bending modulus k_C is typically $10 - 20$ $k_B T$ [9] and k_G is the Gaussian bending modulus. By the Gauss-Bonnet theorem, the second term in the bending energy $k_G K$ contributes only a topological term to the free energy and is therefore irrelevant for describing closed membranes (e.g. see Nakahara [10]). We also wish to note that the Helfrich energy is functionally identical to the Area Difference Elasticity model (ADE) up to the first variation. The effect of an area difference between the two leaflets of the membrane is to produce an effective spontaneous curvature. Incorporation of the parameter C in the Helfrich model can therefore be interpreted to include the contribution of ADE (more detail on this can be found e.g. in Seifert's review of the mechanics of fluid membranes [3]). Note that the $\tfrac{1}{2} k_C C^2$ term in the energy can be absorbed into the definition of the tension.

Shortly after this model was proposed, Jenkins [11] derived the Euler-Lagrange equations for the bulk of the membrane in the presence of a constant external pressure. In a companion paper, Jenkins [12] and more recently Steigmann [13] discussed more abstract models and the general constitutive relations relating force density and couple to local curvature.

C. Membrane forces in the bulk

To derive the equations for local force balance, we introduce the local Lagrange multiplier α, which represents the membrane surface tension. (The area of the membrane is essentially inextensible.) The constrained energy is [11, 14]:

$$E' = E + \int_{\mathcal{M}} \mathrm{d}^2\sigma \, \sqrt{g} \, \alpha. \tag{3}$$

We use the virtual work principle to derive the local forces (see, for example, Landau and Lifshitz [15]):

$$0 = \delta E' - \int_{\mathcal{M}} \mathrm{d}^2 s \, \sqrt{g} \, \vec{f} \cdot \delta \vec{X}, \tag{4}$$

for mechanical equilibrium where $\vec{f}$ is an externally applied force required to cancel the elastic response, $\vec{f}_{\mathrm{int}}$. The derivation of the equilibrium equations is now quite straightforward and analogous to the result found by Jenkins [11]. In the bulk of the membrane the internal elastic response force is

$$
\begin{aligned}
f_{\mathrm{int}}^\perp &= S\alpha - k_C \left[\nabla^2 S - 2 \left(S - C \right) K \right. \\
&\quad \left. + \tfrac{1}{2} \left(S^2 - C^2 \right) S \right],
\end{aligned} \tag{5}
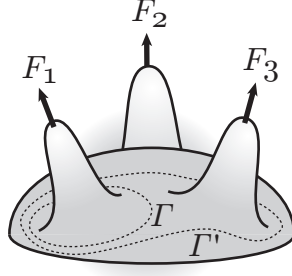$$

$$\vec{f}_{\mathrm{int}}^{\,\parallel} = 0, \tag{6}$$

Figure S1: Membrane with three external forces applied. Dotted lines indicated contours Γ and Γ'. The external forces in these regions can be computed with line integrals.

where ∇^2 is the Laplace-Beltrami operator or, alternatively, the two-dimensional Laplacian on the curved manifold $\mathcal{M}$ and $\perp$ and $\parallel$ denote forces normal to and in the plane of the membrane, repectively. These equations reduce to those derived for constant pressure [11, 14] and are analogous to those derived for generalized theories [12, 13]. There are several points to note about these equations. Since the membrane is assumed to be fluid in-plane, the elastic response is significantly simplified. In the plane of the membrane, only potential-like forces can be supported [12], since shear forces or torques normal to the plane of the membrane will induce flow in the membrane. Furthermore, any shape can be supported by normal forces alone, resulting in a constant tension α. Consequently, we have $\vec{f}_{\text{int}}^{\parallel} = 0$.

D. Membrane forces at the boundary

The approach to calculating these forces is exactly analogous to the calculation in the bulk. The mathematics and results in this section are well known; see, for example, Refs. [16–20]. Let us define two additional unit vectors in the plane of the membrane at the interface: $\vec{N}$ is the outward facing normal and the tangent vector is defined $\vec{T} \equiv \vec{n} \times \vec{N}$. When the membrane has a boundary, the principle of virtual work is

$$
\begin{aligned}
0 &= \delta E' - \int_{\mathcal{M}} \mathrm{d}^2 s \sqrt{g} \, \vec{f} \cdot \delta \vec{X} \\
&\quad - \oint_{\partial \mathcal{M}} \mathrm{d}s \left[\vec{\mathcal{F}} \cdot \delta \vec{X} - \mathcal{L}^N \vec{n} \cdot \nabla_N \delta \vec{X} \right],
\end{aligned} \tag{7}
$$

for mechanical equilibrium, where $\vec{\mathcal{F}}$ is the external force density on the boundary and $\mathcal{L}^N$ is the external normal couple on the boundary required to put the membrane into mechanical equilibrium. The forces are

$$
\mathcal{F}_{\perp}^{\text{int}} = k_C \nabla_{\vec{N}} S - k_G \nabla_T S_{TN} \tag{8}
$$

$$
\mathcal{F}_{\parallel \, i}^{\text{int}} = k_C S_{Ni} (S - C) \tag{9}
$$
$$
- N_i \left[\tfrac{1}{2} k_C (S - C)^2 + \alpha \right] + k_G S_{TN} S_{Ti},
$$

and the couple is

$$
\mathcal{L}_{\text{int}}^N = [k_C (S - C) + k_G S_{TT}]. \tag{10}
$$

E. Total force balance

Noether's theorem guarantees that the total internal force and torque must cancel. (The mathematics and results in this section are well known in the literature [16–20].) The same must be true for the total external force and torque. We will develop the force cancellation explicitly since it will prove quite useful for computing external forces. The total internal force for a membrane with a boundary is

$$
\vec{F}_{\text{int}} = \int_{\mathcal{M}} \mathrm{d}^2 s \sqrt{g} \, \vec{f}_{\text{int}} + \oint_{\partial \mathcal{M}} \mathrm{d}s \, \vec{\mathcal{F}}_{\text{int}} = 0, \tag{11}
$$

where we have integrated by parts to show that the forces cancel. This formalism can be quite convenient for computing external forces applied in a localized region of the membrane $\mathcal{M}'$. Force cancellation implies that the integrated external bulk force is equal to minus that on the boundary $\Gamma \equiv \partial\mathcal{M}'$. The total bulk external force must be equal to the total internal force on Γ:

$$\vec{F}_{\text{ext}} \equiv \int_{\mathcal{M}} \mathrm{d}^2 s \, \sqrt{g} \, \vec{f}_{\text{ext}} = \oint_{\Gamma} \mathrm{d}s \, \vec{\mathcal{F}}_{\text{int}}. \tag{12}$$

For example, the component of the external force due to a constant external pressure p is easily computed explicitly

$$\vec{F}_p = \int_{\mathcal{M}} \mathrm{d}^2 s \, \sqrt{g} \, p \, \vec{n} = \oint_{\Gamma} \mathrm{d}s \, \tfrac{1}{2} p \, \vec{T} \times \vec{X}, \tag{13}$$

where $\vec{F}_p$ is the total pressure force on the surface $\mathcal{M}'$ enclosed by Γ.

These concepts are illustrated graphically in Fig. S1. Consider a fluid lipid bilayer membrane with forces applied as shown in the Figure. The total external force F_1 applied to the membrane can be equivalently calculated as an integral over an areal region $\mathcal{M}'$ or as an integral on the bounding contour Γ:

$$\vec{F}_1 = -\int_{\mathcal{M}'} \mathrm{d}^2 s \, \sqrt{g} \, \vec{f}_{\text{int}} = \oint_{\Gamma} \mathrm{d}s \, \vec{\mathcal{F}}_{\text{int}}. \tag{14}$$

The total external force in the region $\mathcal{M}''$, bounded by contour Γ', can be computed similarly:

$$\vec{F}_1 + \vec{F}_3 = -\int_{\mathcal{M}''} \mathrm{d}^2 s \, \sqrt{g} \, \vec{f}_{\text{int}} = \oint_{\Gamma'} \mathrm{d}s \, \vec{\mathcal{F}}_{\text{int}}. \tag{15}$$

There are two advantages to calculating the external force as a contour integral rather than an integral over an areal region:

1. The internal force $\vec{\mathcal{F}}_{\text{int}}$ on the boundary has been integrated relative to $\vec{f}_{\text{int}}$ therefore it is one order lower in derivatives (third order instead of fourth order) making it more tractable numerically.

2. We may determine the external force without detailed knowledge of the structure of the membrane in the areal region; as long as the boundary has been well-determined experimentally, we may measure the force on the region internal to that boundary.

F. Lagrange multipliers

In the paper, we loosely refer to tension, pressure, and spontaneous curvature as Lagrange multipliers. In mechanics, treating tension and pressure as Lagrange multipliers is justified since the area and the volume are very close to conserved (see Fig. S10, panels A and B). (The area expansion modulus of a lipid membrane is much larger than $k_C S^2$.) The justification for treating these quantities as Lagrange multipliers in statistical physics is more subtle. Even though the membrane is inextensible microscopically, at low tension, volume, area and curvature are hidden in thermal fluctuations leading to an entropic (rather than enthalpic) response to macroscopic area expansion. Furthermore, the spontaneous curvature is certainly not strictly a Lagrange multiplier since the total curvature is not conserved even from a purely mechanical (non-thermal) standpoint. The justification for invoking Lagrange multipliers is that they yield the same first-order variations of the energy (forces) as the rigorous theory. It is only at the second-order variation of the energy that the Lagrange multipliers fail to describe the variation of the energy correctly. For example, to calculate the fluctuations around an equilibrium configuration, the Lagrange multipliers do not suffice. An instructive example is the sphere. In the reservoir (Lagrange multiplier) theory, vesicles are unstable to radial expansion. This is the canonical nucleation problem for bubbles forming in liquid. On the other hand, if the vesicle constraints are treated correctly, these radial expansion modes are infinitely stiff in the mechanics theory.

II. COMPUTATIONAL DETAILS

A. Spline representation

We implemented the vesicle spline representation with the `MATLAB` command `interp1` and the `v5cubic` option. This interpolation scheme was chosen because it was convenient to implement in `MATLAB`. It possesses a number of desirable features: (i) The cubic splines were constructed with C^2 smoothness[1]. (ii) The interpolation method implemented by the `v5cubic` option makes use of basis functions with modest support[2].

B. Calculation of curvature and forces

To implement the calculation of the membrane bending energy, we computed the curvatures from the spline interpolation by finite difference, then numerically integrated the energy. To compute vertex forces, we used a finite difference technique: we deformed the contour by perturbing vertices in the direction of the surface normal and then used Eq. 4 to compute the forces. To compute the integrated forces, we used the generalized Stokes theorem (Eq. 11) and a finite difference strategy of moving the membrane region, defined by the contour, by a slight amount Δz in the axial direction and computing the change in the energy ΔE, giving us a force $F = \Delta E / \Delta z$.

C. Vesicle tracing

In a typical experiment, fifty image frames were captured at each step in an extension series. An extension series usually consisted of between fifty and sixty steps, split between outward and inward movement, with a step size of roughly $1.5\,\mu$m. The integration time was chosen to give sufficient statistics to allow each frame to be traced independently. For the calculations in the main text, we constructed an average image from all the image frames at each step in the extension series. (The additional frames were captured for the analysis of the fluctuations [21].)

The vesicle conformation is represented by a cubic spline. The control points for a typical image are shown in panel A of Fig. S2. The positions of the spline control points in the direction parallel to the membrane contour were chosen by hand for each extension. We attempted a number of automated procedures for choosing the contour length positions of the points but these algorithms were difficult to implement in a robust manner.

The positions of the control points in the direction normal to the membrane contour were fit to the fluorescence profile, employing an empirical model. A good model for the fluorescence profile was found to be a convolution of a structure function with a Gaussian point spread function:

$$I_j(\rho; \rho_0) = \Psi_{\mathrm{PSF}} \otimes I_0(\rho; \rho_0), \tag{16}$$

where I is the intensity at vertex j at position ρ, defined as the distance, normal to the surface, to the axis of symmetry. ρ_0 is the position of the membrane and I_0 and Ψ_{PSF} are the structure function and Gaussian point spread function respectively. The structure function is

$$I_0(\rho; \rho_0) = A\delta(\rho - \rho_0) + A\delta(\rho + \rho_0) + B\Theta_H(\rho + \rho_0)\Theta_H(\rho_0 - \rho), \tag{17}$$

where A and B are constants, δ is the Dirac delta function, and

$$\Theta_H(x) = \begin{cases} 1, & x \geq 0 \\ 0, & x < 0. \end{cases} \tag{18}$$

is the Heaviside step function. The Gaussian point spread function is defined to be

$$\Psi_{\mathrm{PSF}}(x) = \exp(-x^2/2b^2), \tag{19}$$

---

[1] Continuous up to the second derivative. This property was necessary in order to produce well-defined derivatives of the curvature when computing forces.

[2] The interpolated curve over each segment depends on the positions of the two nearest neighboring points on each side. Other options with larger or smaller supports produced curves that differed more noticeably from the vesicle contours.
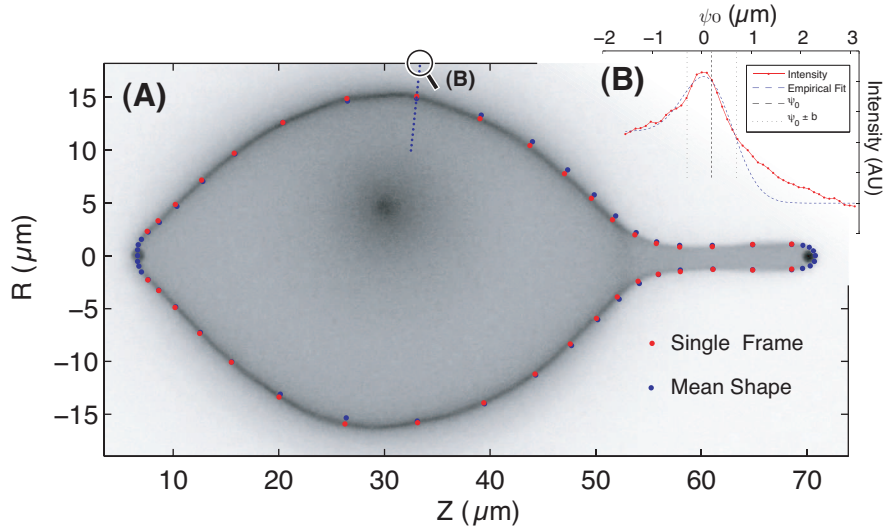
Figure S2: **Capturing the membrane conformation:** A fluorescence image of a vesicle from a force-extension series. The vesicle conformation is represented as a cubic spline. The positions of the control vertices are fit from the fluorescence profile. The red vertices were traced from the fluorescence image shown in the figure; the blue vertices correspond to a trace of the mean of the fifty images at this extension. The vesicle is assumed to be axially symmetric. The localized fluorescence in the body of the vesicle is the result of an internal vesicle. The increase in external osmotic pressure often leads to a budding transition. Note also that the beads are not fluorescent themselves, they appear fluorescent due to the aggregation of lipid there.
(B) Fitting control point positions. The positions of the control points normal to the contour were fit to the fluorescence profile (red curve), employing an empirical model (blue curve). The intensity values shown here were taken from a one dimensional slice of the image, shown as a blue dotted line in panel A.

where b is the point spread width. We have idealized the in-plane membrane as an infinitely thin surface, normal to the plane of focus, with a delta function source of fluorescence. The out-of-focus membrane is represented as a region of uniform intensity (the Heaviside function). A number of more elaborate (non-empirical) models were implemented but this model led to the best approximation of the observed fluorescence profile. The fit to a typical fluorescence profile is shown in panel B of Fig. S2.

In principle the force measurement should not depend on the vesicle representation (the parallel positions or number of the spline control vertices). This representation independence is shown in Fig. S3. Two independent tracings of the vesicle images show that the results for the force on the vesicle do not depend sensitively on the positions of the spline control points, as asserted.

D. Proximal Equilibrium Approximation

Analysis of the fifty image frames at each step in the extension and retraction series yielded a traced contour representing the axisymmetric shape of the vesicle. After determining the membrane structures, the Lagrange multipliers (pressure P, tension α, and spontaneous curvature C) are determined. The condition of (approximate) mechanical equilibrium was used to calculate these three multipliers.

In mechanics, there are three equivalent ways of expressing this equilibrium: at every point on the membrane (i) the energy associated with normal displacement of membrane is minimized, (ii) the force is zero, and (iii) the normal displacement to the equilibrium position is zero. In mechanics, all three of these statements are exactly equivalent. Therefore, for conformations that are dominated by deterministic mechanical forces rather than fluctuations, all three formulations of equilibrium should be equivalent. When fluctuations are important, one must consider the minimization of the free energy which includes the contribution from fluctuations [21].

Although these approaches for determining proximity to equilibrium appear equivalent, we argue that, from an experimental standpoint, using the normal displacements as the objective function (the "distance objective function") is the most powerful. The first advantage of the distance objective function is that the position of vertices is determined in the experiment, not the force or energy at each vertex. It is therefore most natural to describe the experiment in terms of the observables. But most importantly, the distance objective function is least susceptible
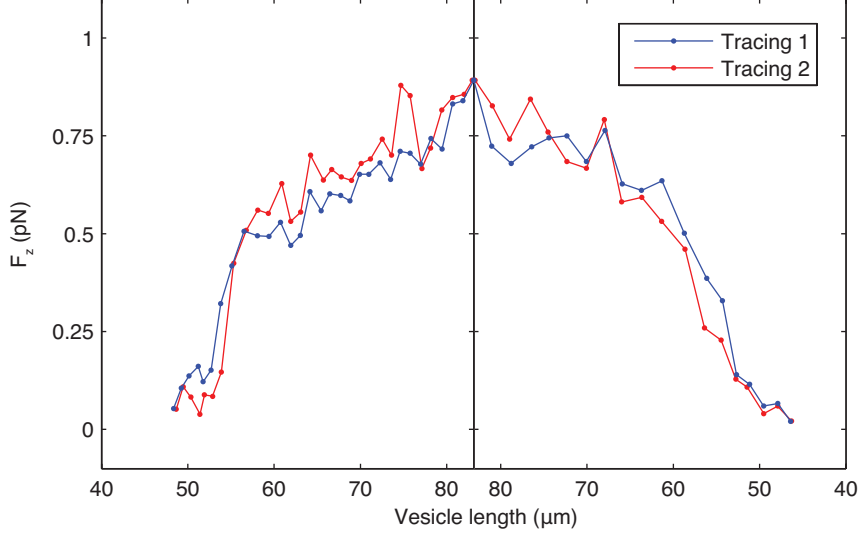
Figure S3: **The conformational force is independent of the tracing representation.** The figure shows two independent tracings of the vesicle extension series; the first tracing is the data shown in the text. It is clear that the two tracings are in quantitative agreement with one another, confirming that our results are not sensitive to a particular choice of spline control points.

to high-frequency (short-contour-length) noise. For configurations that are close to equilibrium, the distance can be computed by multiplying the vertex forces by the stiffness matrix:

$$\psi = -K^{-1}f_\perp. \tag{20}$$

High frequency modes, associated with uncorrelated error in determining the positions of the vertices, can compromise the vertex forces, which depend on a fourth-order derivative of vertex position. But, the error-associated forces are canceled by the forces at neighboring vertices[3]. In essence, to determine the Lagrange multipliers, we wish to high-pass filter these forces to remove the error. Computing the estimated equilibrium displacement provides this desired filtering. High-frequency modes are stiff (have large stiffness eigenvalues) and are therefore suppressed in the estimated equilibrium displacement.

A particular choice of Lagrange multipliers produces a trial configuration of the membrane with control vertices displaced from their positions in the observed experimental shape. These displacements from corresponding vertices in the trial and observed membrane shapes are the estimated equilibrium displacements. To compute the Lagrange multipliers, we apply the Proximal Equilibrium Approximation: we calculate the vertex estimated equilibrium distances, ψ_i, and then minimize the sum of the squares of the equilibrium distances over the entire contour (excluding the regions near the bead attachment points) with respect to the Lagrange multipliers. (This minimization with respect to the spontaneous curvature is illustrated in Fig. S4.) The outcome of the Proximal Equilibrium Approximation analysis is the values of P, α and C as well as the forces at each vertex on the membrane, calculated solely from the shape of the membrane and the membrane bending modulus.

Step by step, the Proximal Equilibirum Approximation is carried out as follows:

1. The observed membrane shape is represented as a discretized mesh: a cubic spline with an associated set of vertices serving as anchor points. We fix the vertices near the points of contact with the trapped beads, where forces are applied.

2. We then compute the vertex forces f_i as a function of the Lagrange multipliers at each vertex i.

3. We calculate the estimated equilibrium displacement ψ_i at each vertex i. For configurations that are close to equilibrium, the distance can be computed by multiplying the vertex force by the stiffness matrix:

$$\psi = -K^{-1}f_\perp, \tag{21}$$

---

[3] The sum of vertex forces, the integrated force, is rather insensitive to the high-frequency noise.
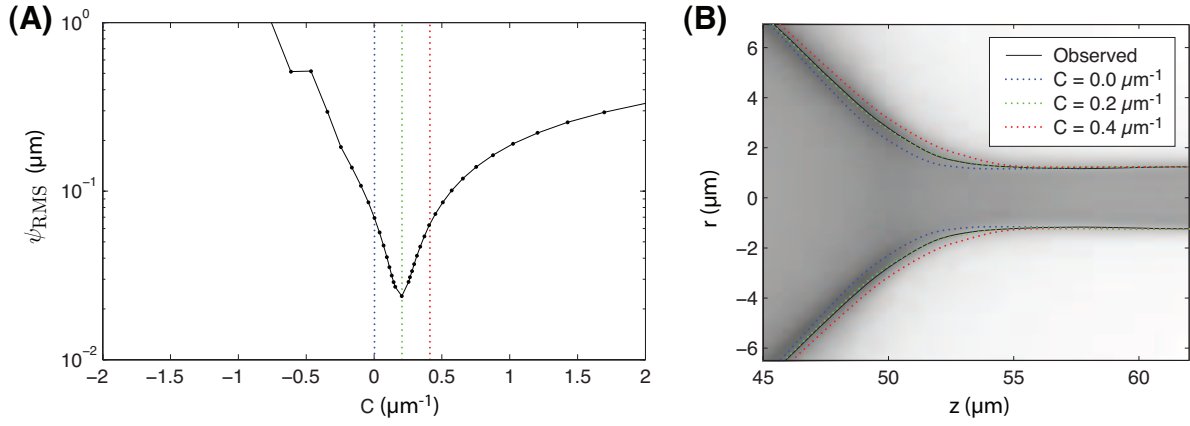
Figure S4: **The determination of C.** The Lagrange multipliers are determined by the Proximal Equilibrium Approximation: the sum of the squared equilibrium displacements (ψ_i) are minimized with respect to a three-dimensional parameter space corresponding to (α, p, C).
Panel A. The plot shows the $\sum_i \psi_i^2$ landscape along the direction of smallest curvature, parameterized by C.
Panel B. The estimated equilibrium shape in the neck for three C values corresponding to the vertical lines in Panel A is depicted. The green curve, corresponding to $C = 0.2 \, \mu\mathrm{m}^{-1}$ (close to the optimal C value), qualitatively matches the observed symmeterized conformation (black).

where K is the stiffness matrix computed by taking the second variation of the Helfrich energy.

  4. We minimize the sum of the squares of the equilibrium displacements for all non-fixed vertices to determine the Lagrange multipliers.

A more complete version of Fig. 2 from the main text, describing the Proximal Equilibrium Approximation, is shown in Fig. S5. Panel B shows the vertex forces for the vesicle depicted in Fig. S2. Force balance in the body of the vesicle is achieved by equilibrium between pressure and tension, whereas in the neck of the vesicle force balance is dominated by equilibrium between tension and elastic forces. The corresponding estimated equilibrium displacements are shown in Fig. S5, panel C.

1. Applicability of the Proximal Equilibrium Approximation

To apply the Proximal Equilibirum Approximation, the conformation must be close to mechanical equilibrium, rather than fluctuation dominated. The key question is: are the fluctuation-induced forces larger than the mechanical forces that result in the mean conformation? Theoretical calculations[4] suggest that this question is resolution dependent but that structures that are reproducible (not fluctuation dominated) do give meaningful results when the Proximal Equilibirum Approximation method is applied. The effect of thermal fluctuations on the consistency of the Proximal Equilibrium Approximation can be tested directly: we generated membrane tracings from both individual image frames as well as from the mean of the fifty images at each step in the extension/retraction series. The analysis of traces from individual image frames results in a distribution of force measurements whose mean can be taken as the value of the force at that step in the experiment. The mean force from the 50 individual tracings varied by an average of 0.07 pN from the value of the force calculated from the traced average image, a value that is small in comparison with other sources of error in the experiment.

A second limitation of the Proximal Equilibrium Approximation is the approximate degeneracy of some membrane conformations with respect to the Lagrange multipliers. Perhaps the most obvious example is the sphere. The Proximal Equilibrium Approximation essentially solves for the Lagrange multipliers by balancing the elastic and constraint forces. For the sphere, there are no elastic forces to balance[5]. Since the elastic forces vanish, there

---

  [4] By perturbing around a flat configuration, we can analyze the contribution of thermal fluctuations to the measured forces. As the resolution of the vertex grid is increased, the force resolution is reduced.
  [5] The fact that the elastic force vanishes for the sphere isn't obvious. The easiest way to see this is to compute the elastic energy of a sphere. In the energy, the factors of R (the radius) from the area and curvature cancel leading to an energy that is scale independent. The radial forces are therefore zero.
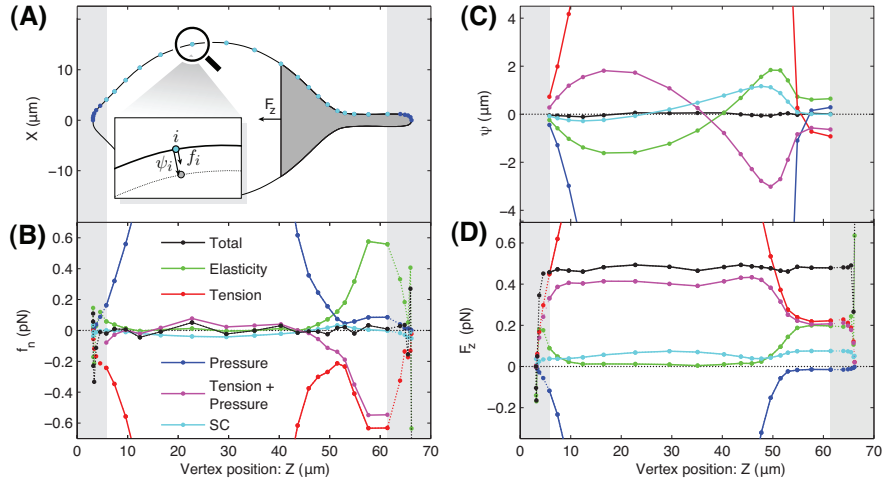
Figure S5: **The Proximal Equilibrium Approximation.**
(A) Vesicle conformation: The axisymmetric vesicle conformation is represented by a cubic spline. The control vertices are drawn as points along the contour. In the panel inset, we show a schematic diagram of the vertex force, f_i, the estimated equilibrium configuration (dotted line), and equilibrium displacement, ψ_i, of vertex i, defined as the normal displacement to the vertex equilibrium position (gray vertex). The summed force at vertex i, F_z^i, is the sum of the z components of the vertex forces in the dark-gray region made by excluding vertices with $z < z_i$. F_z^i is the total force applied by the right hand side of the vesicle in the z direction. In the proximity of the bead attachment points, the membrane structure cannot be resolved with sufficient precision to make reliable force estimates and these regions (light gray on the left and right of both panels) are not analyzed when solving for the pressure, tension and spontaneous curvature of the membrane with the Proximal Equilibrium Approximation.
(B) Vertex force. The vertex force f_i is the sum of components from membrane elasticity, tension, pressure, and spontaneous curvature (SC). In equilibrium, the forces should balance (up to thermal fluctuations) and indeed the total vertex force (black curve) is close to zero for the optimized Lagrange multipliers. In the body of the vesicle, force balance is dominated by tension (red curve) acting to contract the vesicle radius, and pressure (blue curve) acting to expand the radius. In contrast, in the vesicle tether, force balance is dominated by the competition between elasticity (green curve) acting to expand the tether radius, and tension (red curve) acting to contract the tether radius. The induced spontaneous curvature acts principally in the neck of the vesicle where there is a transition between the two regions.
(C) Estimated displacement to equilibrium. Although equilibrium implies force balance, it is difficult to determine the Lagrange multipliers from force balance directly since the vertex force is inherently noisy. Multiplying the vertex force f_i by the inverse stiffness matrix gives the equilibrium displacement ψ_i, the estimated spatial distance to the equilibrium configuration at vertex i. This calculation has the effect of locally averaging the vertex force and suppressing noise (and thermal fluctuations). The distance to equilibrium along the normal to the membrane surface is shown in panel C. We determine the optimal Lagrange multipliers by minimizing the sum of squares of the vertex equilibrium displacements.
(D) Summed force: The summed force is the total force applied by the right hand side of the vesicle. In equilibrium, this force can be computed from the boundary of the region; it is *independent* of the structure of the internal region. This property is of great importance since it implies that we need not resolve the region proximal to the bead attachment. The total integrated force (black) is approximately constant throughout the body of the vesicle as expected, since the forces are applied only at the poles of the vesicle. The force is also shown decomposed into individual contributions from pressure, tension, spontaneous curvature and elasticity with colors as given in panel B.

is a two-dimensional continuum of Lagrange multipliers that satisfy the force balance equations. Obviously, the sphere is a special case, but shapes at the tethering transition point appear to have only a weak dependence on the spontaneous curvature. Uncertainties in the spontaneous curvature appear to dominate the error in conformation force computation. (See Fig. S10.)

A final limitation of the Proximal Equilibrium Approximation is the necessity of guessing and excluding points where external forces are applied when computing the Lagranger multipliers. While the location of the applied forces is obvious in the analysis of deformed vesicles, for biological examples, the position of the applied forces may not be known. Indeed, in many examples, the contacts may be so frequent as to not permit large, force-free regions to be identified and analyzed[6]. On-the-other-hand, in biological applications, the pressure can be completely neglected and

---

[6] In the experiments described in this paper, the deformation incurred by tethered vesicles is so large that the body of the vesicle cannot

the tension and spontaneous curvature may be regulated by the cell or determined using other techniques [22]. If the Lagrange multipliers are known, it is straightforward to compute membrane forces without applying the Proximal Equilibrium Approximation.

E. Error computation for the conformational force

The error in the force computed from the conformation of the membrane was estimated in two ways in our analyses. One method consists of tracing each of the 50 images at each step in the extension/retraction series, applying the Proximal Equilibrium Approximation and then analyzing the resulting distribution of force, pressure, tension and spontaneous curvature measurements. This is the method used to generate the r.m.s. errors on the force shown in the main text.

Another method consists of calculating confidence intervals for the Lagrange multipliers and then deriving the error in the force based on those uncertainties. This can be done by standard methods; see, for example, Bevington and Robinson [23], whose analysis we follow here. The Proximal Equilibrium Approximation amounts to a non-linear least squares fit of the membrane contour given values for the pressure, tension and spontaneous curvature to the observed membrane contour. The χ^2 goodness-of-fit parameter in the Proximal Equilibrium Approximation is:

$$\chi^2 = \sum_i \frac{1}{\sigma_i^2} \left[y_i - y_{\text{obs}} \right]^2, \tag{22}$$

where σ_i is the uncertainty in the position of vertex i in the direction normal to the membrane contour, y_{obs} is the observed position of the vertex in the normal direction and y_i is the position of the ith vertex given parameter values P, α and C. The uncertainty in the normal positions, σ_i, was essentially constant for each of the vertices in a given image from our experiments. In the neighborhood of the minimum χ^2 value found by the Proximal Equilibrium Approximation, we may use a Taylor expansion of our fitting function, y_i, to find:

$$\Delta a_j = \epsilon_{jk} \beta_k \tag{23}$$

where Δa_j is the uncertainty on the jth parameter, ϵ_{jk} is the error matrix and β_k is the derivative of χ^2 with respect to the kth parameter. This was the technique used in generating the errors shown as dotted lines on the plots of pressure, tension and spontaneous curvature in Fig. S10 below. More generally, after finding the optimal point in χ^2 space, we may calculate the χ^2 values in the neighborhood of this point and find contours in parameter space where χ^2 increases by a given amount to find arbitrary confidence intervals on the parameters. We found that using the χ^2 method of estimating confidence intervals on the parameters predicted larger errors than the r.m.s. method from the 50 images at each step in the experiment.

---

be treated as a reservoir with constant Lagrange multipliers. In most biological systems of interest, the size of the remodeled regions is small in comparison with the size of the cell. For cellular-scale membrane deformations, membrane force computations are unlikely to be of interest since it is not the membrane mechanics which dictates the shape, but the underlying structure of the cytoskeleton.
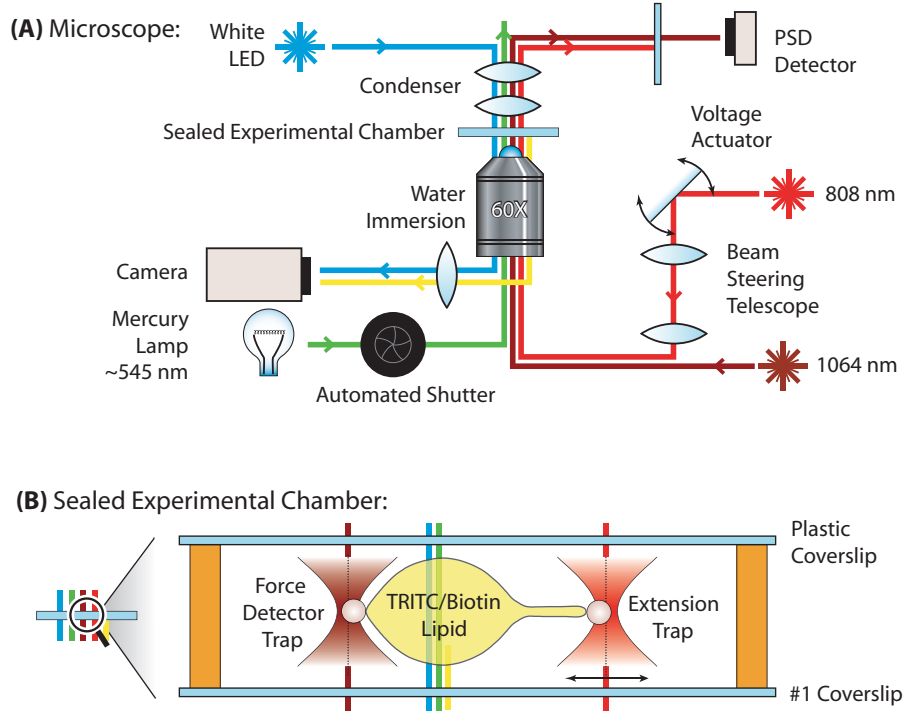
III. EXPERIMENTAL DETAILS

A. Optical setup

The measurements were performed using a custom apparatus comprised of two optical traps integrated with a fluorescence microscope. (See panel A of Fig. S6 for a schematic drawing of the vesicle force-extension apparatus.) Forces were applied to vesicles by binding streptavidin-coated 1 μm beads to DOPC giant unilamellar vesicles doped with biotin and TRITC. The vesicles were composed of 99% DOPC, 0.5% DOPE-biotin and 0.5% DOPE-TRITC by molar fraction[7].

A 1064 nm trap was used as a force detector. The beam deflection was detected in the back focal plane by a position sensitive detector (PSD) [1]. A second 808 nm trap was employed to deform the vesicles. This second color trap was used to avoid crosstalk between the deflection and force detection beams at the PSD. The position of the 808 nm trap was varied using a beam steering telescope driven by a computer controlled voltage actuator.

The radius of a typical vesicle was approximately 15 μm. In order to avoid membrane contact with the surface, experiments were performed at a distance of roughly 100 μm from both surfaces of the experimental chamber. To trap beads at these long working distances, it was necessary to employ a 60X water immersion objective. The trap stiffness was nearly independent of the working distance. The vesicles were imaged using TRITC fluoresence, excited by a mercury lamp. Bead fishing was performed using brightfield microscopy, lit by a white LED. Vesicles were imaged using a Hamamatsu ORCA 285 camera.

The vesicle extensions were performed in a two-input flow chamber. After blocking the chamber with BSA, the vesicle solution was pipetted into one of the input ports to fill the chamber. This input port was then sealed and the buffer was allowed to slowly evaporate from the unsealed input port, increasing the external osmotic pressure. When the vesicles became sufficiently soft, a charge of streptavidin-coated 1 μm beads was pipetted into the remaining input port and the port was sealed. The flow chamber is depicted schematically in panel B of Fig. S6.

Figure S6: **(A) Experimental apparatus schematic drawing.** The measurements were performed using a custom setup composed of two optical traps integrated with a fluorescence microcope. The beam deflection from the 1064 nm trap was detected in the back focal plane by a position sensitive detector (PSD). A second 808 nm trap with a beam-steering telescope were employed to deform the vesicles.
(B) Experimental chamber detail. The experiments were performed in a sealed two-input flow chamber. Forces were applied to vesicles by binding streptavidin-coated 1 μm beads to DOPC giant unilamellar vesicles labeled with biotin and TRITC. Images of the fluorescently labeled lipid were analyzed to extract dynamic information about thermal membrane fluctuations as well as calculate the static elastic forces.

The diffusion constant of beads in the sucrose solution used in this experiment was measured by tracking the diffusion of 1 μm beads, with no lipid present, in the sealed two-input flow chamber described above. A custom software package, kindly provided by Robert Bao, was used to analyze the time-series images of bead diffusion. The diffusion constant for water was measured to be 0.88 cP and that of the bead solution to be 0.98 cP.

B. Optical trap force measurement

Measurement of piconewton forces with optical traps is a well-studied subject, reviewed e.g. in Neuman and Block [2]. Note that we have checked that the size of the fluctuations (the spring constant) remains nearly constant during vesicle extension experiments implying that the presence of the vesicle does not affect the trap stiffness and the trap remains close to the linear regime. The mean and variance of the voltage are shown in Fig. S7.
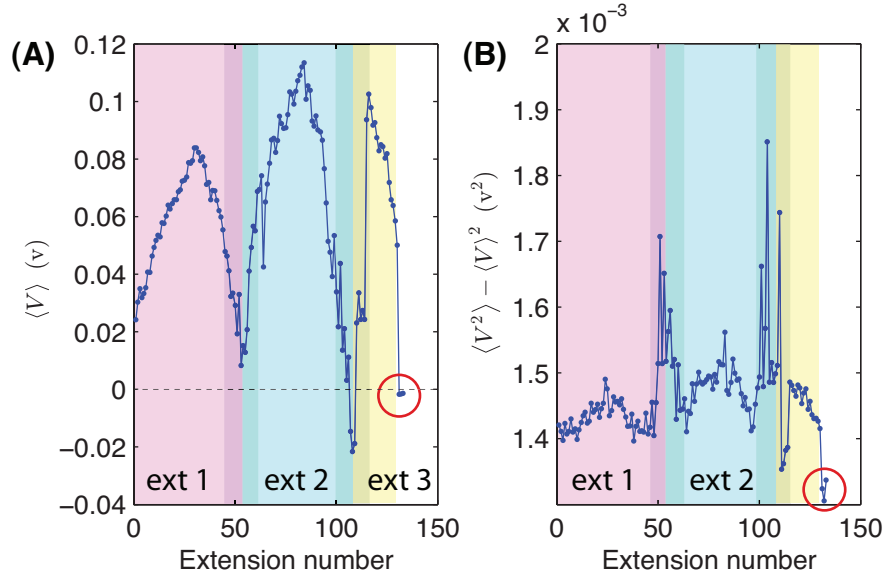

Figure S7: **Panel A:** The mean PSD voltage plotted versus extension number for a three extension data set. The trap deflection (and force) are proportional to the PSD voltage. The last three circled points are the zeros for the experiment with beads unattached to the vesicle. The initial points on the trace correspond to beads bound to the vesicle, but without extension. Binding the vesicle causes an anomalous force due to scattering of light. See discussion in the caption of Fig. S8.
Panel B: The voltage variance versus extension number. The voltage variance is inversely proportional to the trap stiffness. Note first that the voltage variance is stable relative to its magnitude throughout the extension. (The data has been plotted to accentuate variations by not including zero on the y axis.) As the force is increased in the first extension, the voltage variance is increased slightly, corresponding to a slight reduction in the trap stiffness, as would be expected due to the large-deflection non-linearity in the trap. Two larger features are visible in the voltage variance at extension numbers 65 and 110. These features are the result of changes in the local structure of the vesicle surrounding the bead. See discussion in the caption of Fig. S8.

1. Vesicle-induced force artifacts

Although the vesicle does not significantly affect the trap stiffness, it does affect the DC offset of the PSD. If the trap is zeroed without contact with the vesicle, the presence of the vesicle in the beam scatters light, leading to an
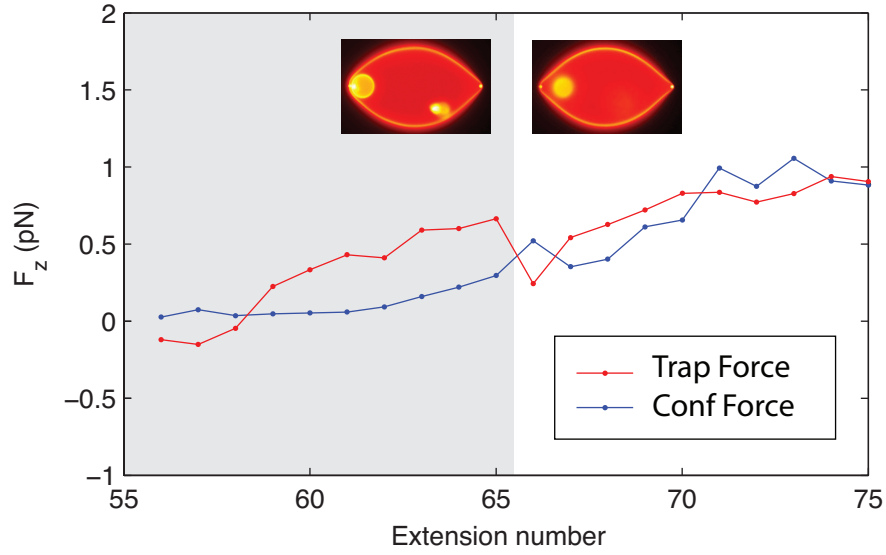
Figure S8: **A limitation of measuring trap forces in the presence of a vesicle.** The vesicles themselves scatter the trapping beam, which can result in the detection of anomalous forces. In the figure above, we depict the most compelling evidence for this effect. At the beginning of this data set, an internal vesicle is bound to the lipid aggregate surrounding the bead. Between extension numbers 65 and 66, the vesicle is released and diffuses into the body of the outer vesicle. This release causes a precipitous drop in the detected trap force (black curve). For reference purposes, we have also plotted the force calculated from the membrane conformation (blue curve). A similar offset in force is observed upon attachment of the force detection bead to the vesicle. Rigorously, this implies that at best we can detect relative forces, not absolute forces. Similar anomalies occur when the vesicle becomes tethered at the detection bead, due to a dramatic change in local vesicle structure. The most reliable force traces resulted from vesicles tethering at the extension bead. In spite of these complications, the trap stiffness was not significantly affected by the vesicle.

offset voltage at the PSD. It was therefore necessary to assume a zero on bead contact. The beads were bound to the membrane by squeezing the vesicle between the trapped beads.

We also discovered that changes in the vesicle conformation in proximity to the bead could also lead to force artifacts. The evidence for this effect is discussed in Fig. S8. Data sets where the vesicle tethered on the pole opposite from the force sensor did not appear to show these anomalous forces, presumably because the local vesicle conformation was not appreciably changed by deformation.

We also note that the trapping force is susceptible to drift in the sub-piconewton regime. Due to the competing effects of drift and systematic uncertainties related to membrane-induced beam scattering, the most meaningful comparisons between the conformational force and the trapping forces are differences between conformations separated by a few extension steps since the membrane-induced scattering is similar and the drift between adjacent steps is smaller than between measurements taken ten to twenty minutes apart. As a practical matter of reducing the influence of drift and low-tension vesicle structure induced force anomalies, the DC offset was calculated by minimizing the difference between the trapping force and conformational force at high force.

IV.   ADDITIONAL DATA

In this section, we provide a more extensive presentation of the experimental data. We present both the vesicle structures and the Lagrange multipliers computed for the extension series shown in the main text. In Section IV B, we present force-extension data from other vesicle extension series.

In Fig. S9, we show a complete set of traced membrane conformations for the vesicle force extension curve discussed in the main text. Under extension, the vesicle undergoes a shape transition to a tethered conformation. The body of the vesicle is supported by tension-induced contractive forces which balance the outward force of pressure. But, as the radius of curvature shrinks at the tether neck, the tension forces increase as R^{-1}, overcoming the outward pressure. The tether neck radius shrinks until the outward-acting elastic force, which scales like R^{-3}, stabilizes the conformation. This force cancellation is illustrated explicitly in Fig. S5 in Section II D.
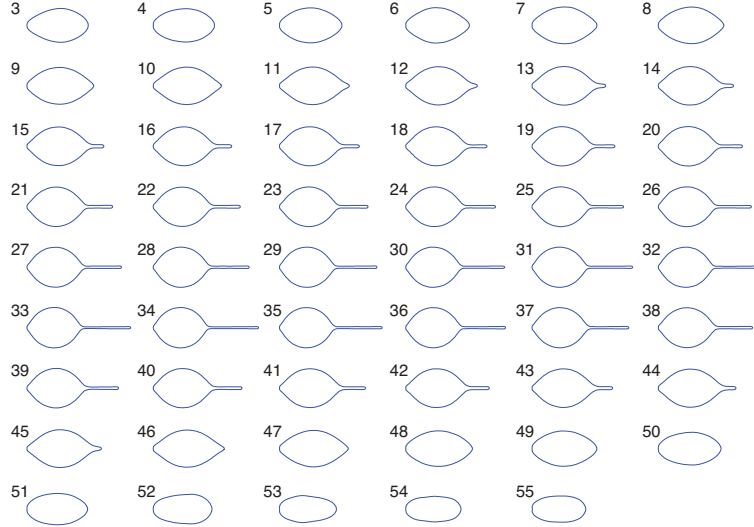

Figure S9: **The vesicle conformations:** In the figure above we show the symmeterized mean vesicle conformations with the corresponding extension numbers for the data analyzed in the text.

A.   Lagrange multipliers

As described in Sect. II D, the Lagrange multipliers for each configuration are determined by applying the *Proximal Equilibrium Approximation*. Although we refer to these quantities as Lagrange multipliers, they have a simple physical interpretation: P, α, and C are the pressure, tension, and spontaneous curvature respectively. From a macroscopic mechanics perspective, the pressure and tension are essentially constraint forces since the membrane area and volume are essentially inextensible at the forces applied in this experiment. Spontaneous curvature is more subtle. Two important effects contribute to the spontaneous curvature: (i) the number of lipid molecules in each leaflet relative to the leaflet area, and (ii) asymmetries in the composition or solvent environment of the two leaflets. The *Area Difference Elasticity* model (ADE) describes how the leaflets expand and contract in order to accommodate the area difference between bilayers [3]. We found that the values of all three of the Lagrange multipliers evolved with the vesicle conformation. These results are shown in Fig. S10 where the Lagrange multipliers are plotted as a function of the extension number. In Fig. S11, we plot the effective constitutive relations for the vesicle.

1.   Pressure and tension

At the beginning of the extension (the end of the retraction) in Fig. S10, there is a steep rise (drop) in the apparent volume and area of the membrane contradicting the claim that the vesicle volume and area are incompressible. This is entropically induced elasticity: although the actual volume and area of the membrane are nearly incompressible, some volume and area are hidden in the thermal membrane undulations. In Fig. S11, the fluctuation-dominated regime is clearly visible, corresponding to the "constant" tension and pressure regimes. In the high-tension limit,
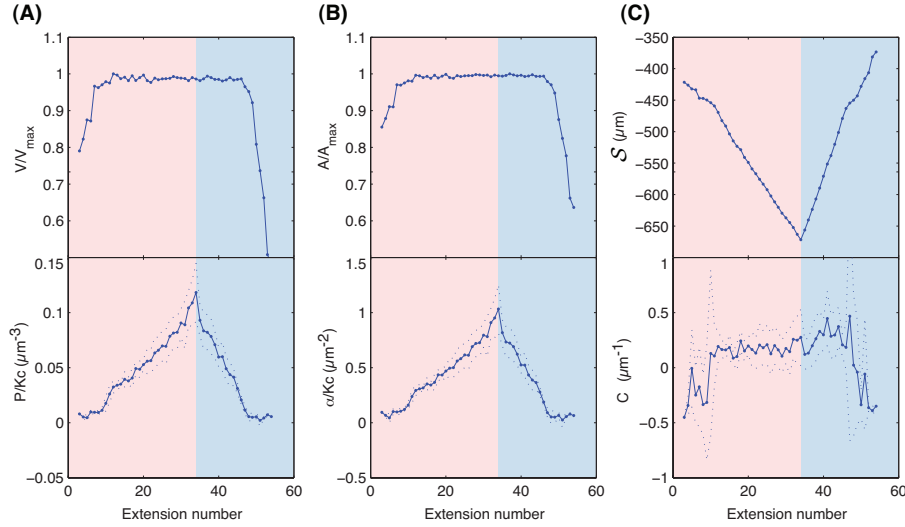
Figure S10: **Tension, pressure and spontaneous curvature of a tethered vesicle.** In this figure we plot the estimated pressure p, tension α and spontaneous curvature C as a function of extension number for an extension (pink region) and contraction (blue region) of a vesicle. The volume V, area A and integrated curvature $\mathcal{S}$ are also shown.
Panels A and B: In the top panes of Panels A and B, the apparent volume and area of the mean conformation are plotted versus extension number. The volume and area of the membrane are fixed, therefore the change in apparent volume and area upon extension and contraction is the result of volume and area hidden in fluctuations from the mean, cylindrically-symmetric conformation. In the lower panes of Panels A and B, the vesicle pressure and membrane tension are plotted versus extension number as determined by PEA, respectively. The pressure and tension rise steadily with tether extension and are peaked, as expected, at the maximum extension.
Panel C: The Integrated curvature and spontaneous curvature as a function extension number. The spontaneous curvature is predicted to be a linear function of the integrated curvature by the ADE theory. This linear relationship is not observed and explanations for the failure of the ADE model to predict the spontaneous curvature are discussed in the text.

little membrane remains in membrane undulations and the tension and pressure can be interpreted as constraint forces. This regime is characterized by the constant area and volume at high tension as shown in Fig. S11.

2. Spontaneous curvature

The evolution of the spontaneous curvature is perhaps the least intuitive and understood of the Lagrange multipliers. The ADE theory predicts the dependence of spontaneous curvature on membrane deformation [3–5]:

$$C = -K_{\mathrm{ADE}}\left(\langle S\rangle_{\mathcal{M}} - S_0\right), \tag{24}$$

where K_{ADE} is a non-local bending modulus and

$$\langle S\rangle_{\mathcal{M}} \equiv \mathcal{S}A^{-1} = A^{-1}\int_{\mathcal{M}} \mathrm{d}^2\sigma\ S, \tag{25}$$

is the mean summed curvature over the deformed vesicle and S_0 is a constant. If the membrane is initially equilibrated by the slow processes of lipids flipping between leaflets, we would expect S_0 to be zero for the undeformed vesicle. In Fig. S11, this simple linear dependence on the mean summed curvature is not observed.

Unfortunately, there are a number of important considerations that may complicate the interpretation of the measured spontaneous curvature. (i) The relative error in the determination of the spontaneous curvature is larger than the other two Lagrange multipliers. (ii) In the fluctuation-dominated regime, the *Proximal Equilibrium Approximation* is problematic since the thermal undulations are large. Furthermore, the mean summed curvature reported in Fig. S11 does not account for the curvature in fluctuations, whereas mean summed curvature in Eq. 24 does include fluctuations. Like the membrane area, a considerable amount of the curvature is in membrane undulations at low tension. The summed mean curvature in the averaged conformation becomes more negative as the membrane is deformed, but as the tension is increased with membrane deformation, the curvature in undulations becomes less
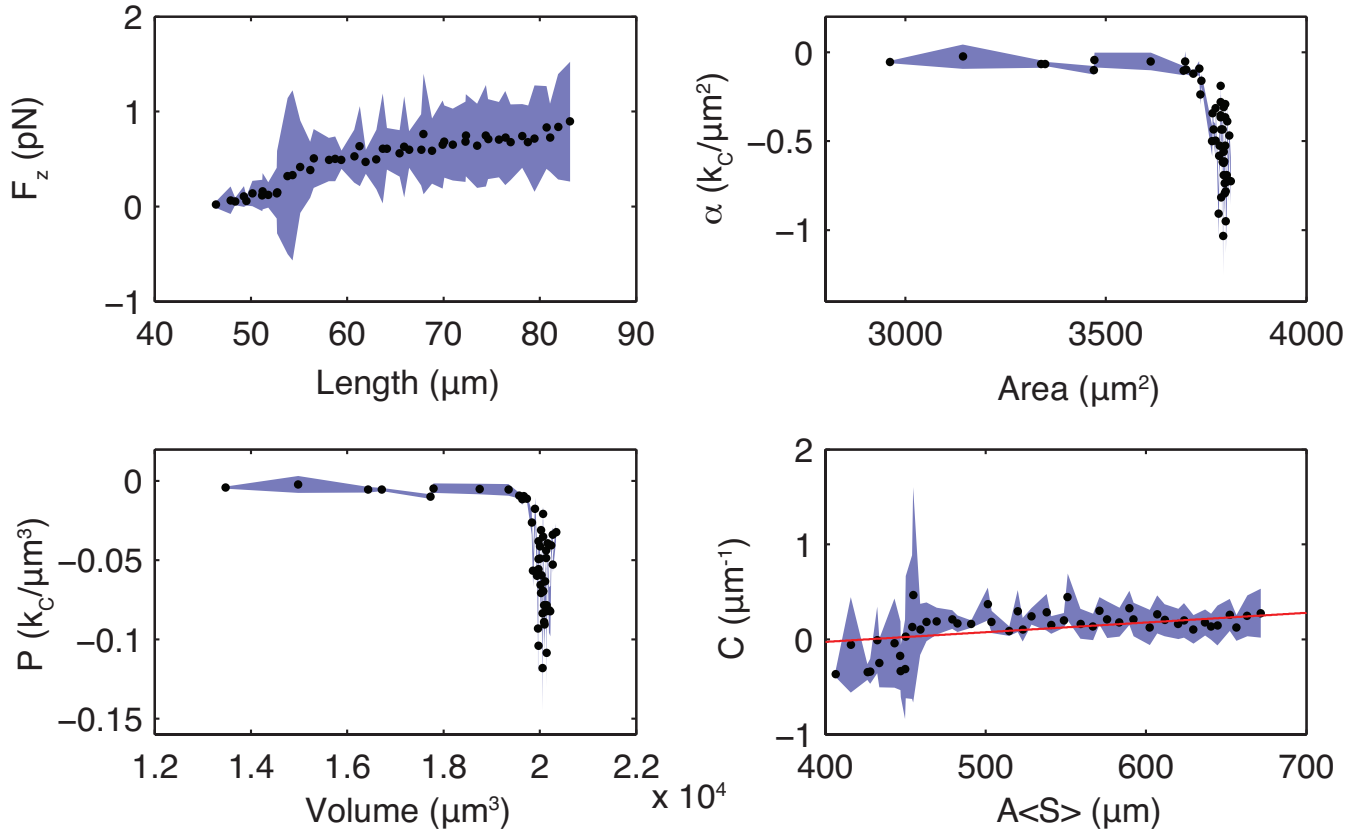
Figure S11: **Effective constitutive relations for a tethered vesicle.** In this figure we plot force versus length, tension versus area, pressure versus volume and spontaneous curvature versus integrated curvature for the vesicle shown in the main text. The black points indicate measured values and the blue regions show the corresponding errors in the ordinate variable. We note that the error in the right-most points on the the tension and pressure plots, which appear here to be small and approximately constant, are actually dominated by the errors in area and volume, respectively, which are not shown. The predicted theoretical curve according to Eq. 24 (which did not require a fit) is shown in red for C versus integrated mean curvature.

negative as it approaches zero. Therefore, the effect of entropy makes the interpretation of the dependence of the spontaneous curvature on the mean summed curvature problematic. (iii) Finally, there is also an important experimental consideration with regards to Eq. 24. This prediction depends on the assumption that the number of lipids in each bilayer is constant. Although the process of lipid transfer between leaflets is thought to be too slow to affect our experiments, all the vesicles in our experiments were functionalized and the osmotic pressure was lowered significantly, inducing budding transitions in many of the vesicles. These transitions may lead to defects in the membrane wall that could affect the lipid number either by allowing faster interchange between leaflets or by the opening of small, partially budded features on the membrane surface. Also, the effect of the optical bead interaction with the membrane cannot be ignored. In our experiments we observed the build up of fluorescence around the beads as the experiment progressed. While the fluorescent lipid may have originated from small vesicles in solution, it may also have been aggregated from the body if the vesicle itself, upsetting the fine balance of the lipid number in the body of the vesicle. Although it is difficult to draw any definite conclusions from the spontaneous curvature data, this data suggests that we may still not understand the nature of spontaneous curvature at physiological tensions.

B. Other extension series

In this section we present force measurements from other vesicles that were not included in the main text. In each plot, the red curve is the force measured from the optical trap and the blue curve represents the force measured from the conformation of the membrane using the Proximal Equilibrium Approximation.
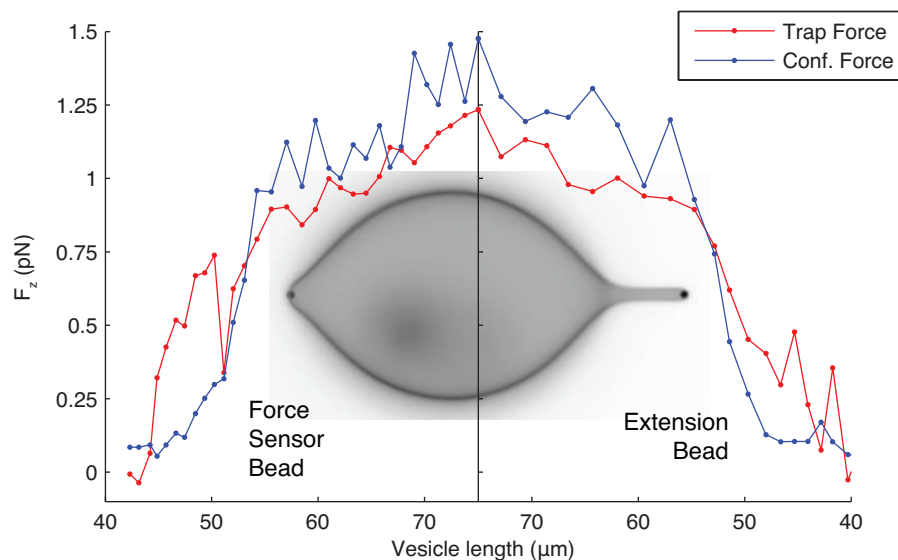
Figure S12: **Data set 2:** Anomalous forces due to light scattered by the membrane itself are apparent in the first few steps of this extension in the trap force; see Fig. S8 and discussion for more details.
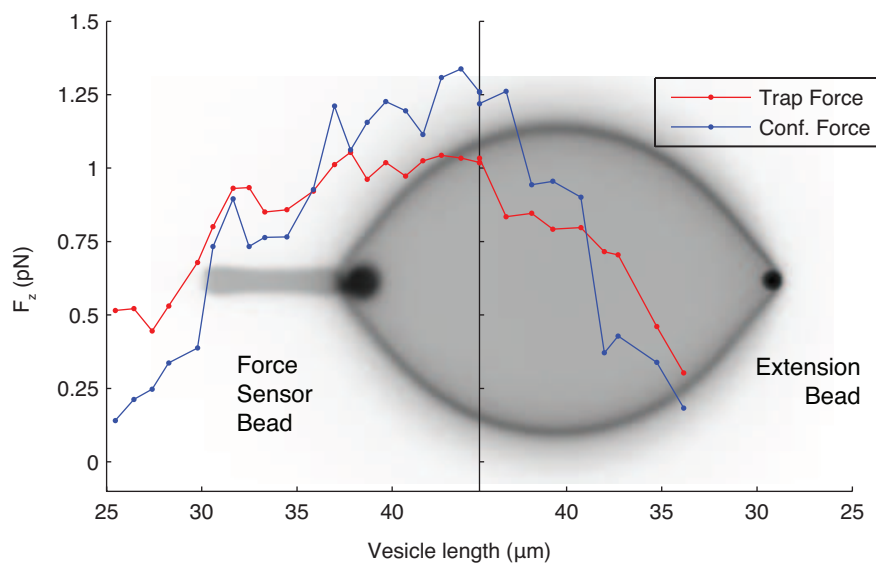

Figure S13: **Data set 3:** Anomalous forces due to light scattered by the membrane itself are apparent in the trap force. We found that data sets where the vesicles tethered on the extension side resulted in the best quantitative agreement with the conformational force. This is probably a result of the dramatic membrane conformational changes at the tethering pole which, in turn, lead to changes in the membrane induced scattering.
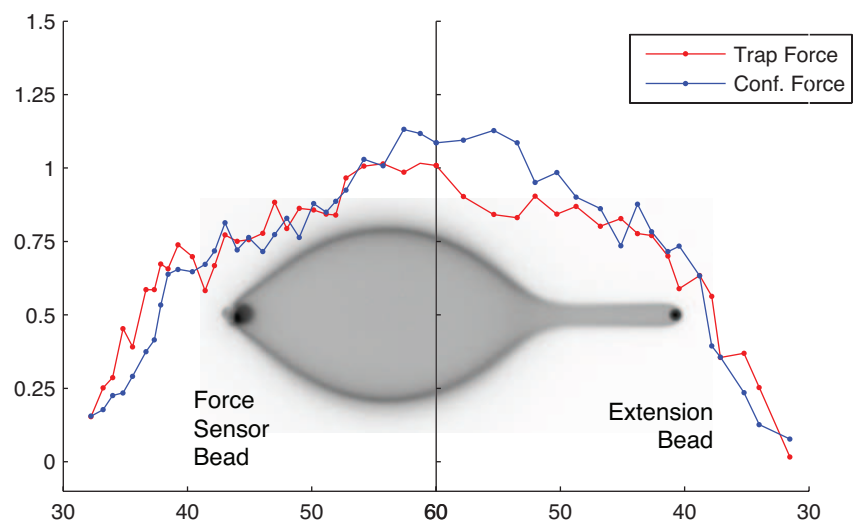
Figure S14: **Data set 4:** This figure shows excellent agreement between the trap and conformational force.
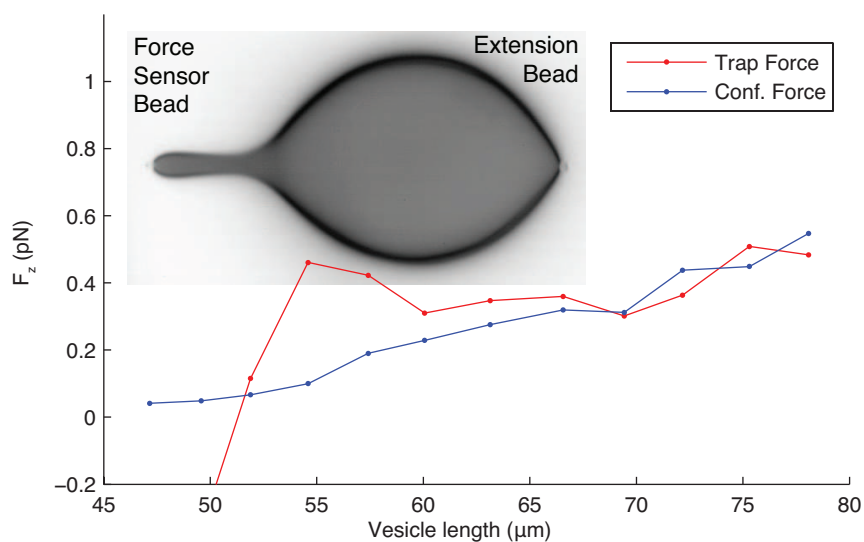

Figure S15: **Data set 5:** This figure shows an extreme example of the anomalous trapping forces induced by large-scale membrane conformational changes at the force sensor bead.
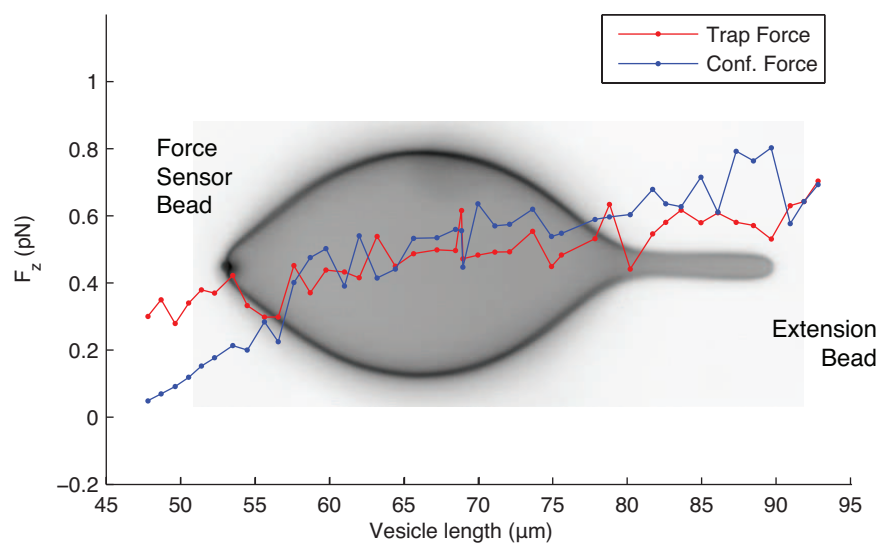
Figure S16: **Data set 6:** This figure shows excellent agreement between the trap and conformational force for higher forces.
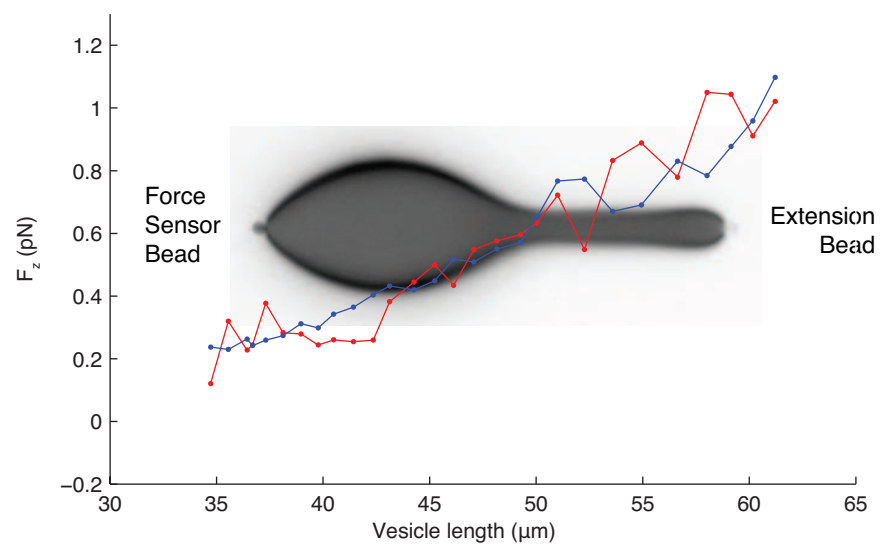

Figure S17: **Data set 7:** This figure shows excellent agreement between the trap and conformational force.

[1] K. Visscher, S.P. Gross, and S.M. Block. Construction of multiple-beam optical traps with nanometer-resolution position sensing. *Selected Topics in Quantum Electronics, IEEE Journal of*, 2(4):1066–1076, Dec 1996.

[2] Keir C Neuman and Steven M Block. Optical trapping. *Rev Sci Instrum*, 75(9):2787–2809, 2004.

[3] U. Seifert. Configurations of fluid membranes and vesicles. *Advances in Physics*, 46(1):13–137, Jan-Feb 1997.

[4] R E Waugh, J Song, S Svetina, and B Zeks. Local and nonlocal curvature elasticity in bilayer membranes by tether formation from lecithin vesicles. *Biophys J*, 61(4):974–82, 1992.

[5] L Miao, U Seifert, M Wortis, and HG Dobereiner. Budding transitions of fluid-bilayer vesicles: The effect of area-difference elasticity. *Physical Review E. Statistical Physics, Plasmas, Fluids, and Related Interdisciplinary Topics*, 49(6):5389–5407, 1994.

[6] W Helfrich. Elastic properties of lipid bilayers: theory and possible experiments. *Z. Naturforsch.*, 28(11):693–703, 1973.

[7] P B Canham. The minimum energy of bending as a possible explanation of the biconcave shape of the human red blood cell. *J Theor Biol*, 26(1):61–81, 1970.

[8] E A Evans. Bending resistance and chemically-induced moments in membrane bilayers. *Biophysical Journal*, 14:923–931, 1974.

[9] W Rawicz, K C Olbrich, T McIntosh, D Needham, and E Evans. Effect of chain length and unsaturation on elasticity of lipid bilayers. *Biophys J*, 79(1):328–339, 2000.

[10] Mikio Nakahara. *Geometry, topology, and physics*. Institute of Physics Publishing, 1990.

[11] J T Jenkins. Equations of mechanical equilibrium of a model membrane. *SIAM J. Appl. Math.*, 32(4):755–764, 1977.

[12] J T Jenkins. Static equilibrium configurations of a model red blood cell. *J Math Biol*, 4(2):149–69, 1977.

[13] D J Steigmann. Fluid films with curvature elasticity. *Archive for Rational Mechanics and Analysis*, 150(2):127–152, 1999.

[14] OY Zhong-can and W Helfrich. Bending energy of vesicle membranes: General expressions for the first, second, and third variation of the shape energy and applications to spheres and cylinders. *Phys Rev A*, 39(10):5280–5288, 1989.

[15] L D Landau and E M Lifshitz. *Theory of Elasticity*. Pergamon Press, 3rd english ed. revised and enlarged by e.m. lifshitz, a.m. kosevich, and l.p. pitaevskii (soft) : edition, 1986.

[16] R. Capovilla, J. Guven, and J. A. Santiago. Deformations of the geometry of lipid vesicles. *Journal of Physics A-Mathematical and General*, 36(23):6281–6295, Jun 2003.

[17] R. Capovilla and J. Guven. Stress and geometry of lipid vesicles. *Journal of Physics-Condensed Matter*, 16(22):S2187–S2191, Jun 2004.

[18] Martin Michael Muller, Markus Deserno, and Jemal Guven. Balancing torques in membrane-mediated interactions: exact results and numerical illustrations. *Phys Rev E Stat Nonlin Soft Matter Phys*, 76(1 Pt 1):011921, 2007.

[19] Markus Deserno, Martin Michael Muller, and Jemal Guven. Contact lines for fluid surface adhesion. *Phys Rev E Stat Nonlin Soft Matter Phys*, 76(1 Pt 1):011605, 2007.

[20] J. B. Fournier. On the stress and torque tensors in fluid membranes. *Soft Matter*, 3(7):883–888, 2007.

[21] E Peterson, H J Lee, R Phillips, W Klug, and P Wiggins. In preparation.

[22] Arpita Upadhyaya and Michael P Sheetz. Tension in tubulovesicular networks of golgi and endoplasmic reticulum membranes. *Biophys J*, 86(5):2923–8, 2004.

[23] Philip R Bevington and D. Keith Robinson. *Data reduction and error analysis for the physical sciences*. McGraw-Hill, 3rd edition, 2003.